Immersed boundary method based Lattice Boltzmann method to simulate complex geometry flows

D. J. Chen, K. H. Lin and C. A. Lin
Department of Power Mechanical Engineering, National Tsing Hua University
Hsinchu 300, TAIWAN
E-mail: calin@pme.nthu.edu.tw

Abstract - In this paper, the lattice Boltzmann method is combined with the immersed boundary technique to simulate complex geometry flows both with stationary and moving boundaries. The complex geometry is represented by Lagrangian markers and forces are exerted at the Lagrangian markers in order to satisfy exactly the prescribed velocity of the boundary. This force at the Lagrangian markers is then distributed to the Eulerian grid by a well-chosen discretized delta function. With the known force field in the Eulerian grid to mimic the boundary, the lattice Boltzmann method is used to compute the flow field where the complex geometry is immersed inside the Cartesian computational domain. The proposed method is examined by computing lid driven cavity flow and flows over both stationary and moving cylinder. All the numerical results agree well with the analytical solution or the benchmark solution, and the Galilean invariance is satisfied.

Keywords— **Immersed boundary method; lattice Boltzmann method.**

I. INTRODUCTION

Historically, the lattice Boltzmann method originated from lattice gas automata [1], a discrete particle kinetics utilizing a discrete lattice and discrete time. While a particle in the lattice gas automata model is represented by a Boolean number, the single-particle distribution function in the lattice Boltzmann method is represented by a real number. Even though the lattice Boltzmann method appears to be rather different from its lattice gas automata counterpart because various approximations, such as the linearization of the collision operator [2] and the Bhatnagar-Gross-Krook (BGK) [3]-[4] approximation [5], has been applied, the theoretical framework of the lattice Boltzmann method nevertheless rests upon the Chapman-Enskog analysis of the lattice gas automata.

Major advantages of the lattice Boltzmann method are due to the fact that it is explicit, easy to implement, and natural to parallelize. The lattice Boltzmann method consists of two essential steps: collision step and streaming step. The collision step models interactions among fluid particles. The streaming step simply moves particles from one lattice to the other according to their velocities. It has been shown that at low Mach numbers the lattice Boltzmann method solves fluid problems with second order accuracy both in space and time [6][7],. The incompressible Navier-Stokes equations can be obtained in the nearly incompressible limit of the lattice Boltzmann method.

To handle a moving curved boundary by the lattice Boltzman method, Filippova and Hanel [8] proposed a method using a simple linear interpolation between a fictitious equilibrium distribution function and a well-chosen near-boundary distribution function. The weighting factor of the interpolation is determined by the distance between the boundary and the near-boundary lattice. Mei et al. [9] further improved its numerical stability. Lallemand and Luo [10] combined the bounce-back scheme and interpolation scheme to treat a moving curved boundary by the lattice Boltzmann method. The bounce-back scheme simulates a stationary boundary, and an additional term is added to implement a moving boundary. This treatment is an extension of that proposed by Bouzidi et al. [11].

In computational fluid dynamics, the immersed boundary method is another convenient approach to treat fluid flows involving complex boundary, though it was formulated mostly within the Navier-Stkes equation framework. The immersed boundary method proposed by Peskin [12] has been applied successfully to blood-valve interaction and other biological problems. Although the immersed boundary method is developed to handle mostly the fluid problem with elastic structure, it has also been used to simulate the flow with rigid boundary or structure. Lai and Peskin [13] proposed a formally second-order accurate immersed boundary method and applied to simulate the flow past a rigid cylinder. Because stiff springs are used to connect the boundary points to their target positions,the problem becomes very stiff which has the consequence of the small time step.

Goldstein et al.[14] [15] proposed the virtual boundary method to simulate the flow with solid boundary within the spectral method framework. Similar to the immersed boundary method, force is exerted at the solid boundary and is calculated according to the difference between the predicted velocity and the actual velocity of the boundary. However, in order to prevent the generation of the spurious oscillations in simulating the start-up flow around a cylinder, the magnitude of the CFL number has to be kept below $O(10^{-2})$. Later on, Saiki and Biringen [16] further improved the work of Goldstein et al. and used the area-weighted average function to interpolate the fluid velocity to the boundary points and distribute the boundary force back to grid points. Mohd-Yusof [17] proposed a different approach to evaluate the required force to impose the no-slip condition at the immersed boundary. The required

force is directly computed from the momentum equations so that the time step can be larger than the previous methods. This direct momentum forcing is applied either inside the body or on the surface. Fadlun et al. [18] further extended the work of Mohd-Yusof to a finite-difference formulation on a stagger gird system, and showed that the direct forcing suggested by Mohd-Yusof is more efficient than the feedback forcing of Goldstein et al.

Body force within the lattice Boltzmann equation has been investigated. Buick and Greated [19] discussed four different implementations of gravity in the lattice Boltzmann method. The first one is to express the gravity in terms of the gravitational potential: $-\rho \bigtriangledown \phi$, and the Navier-Stokes equation incorporating the body force is expressed in the same where the potential is absorbed into the pressure: $p + \rho\phi$. Second one is to consider the momentum change produced by the body force, and to replace the macroscopic velocity in the equilibrium distribution function by $\vec{u} + \vec{F}\triangle t/\rho$. Third one is to add an additional term to the collision operator. Fourth one is to combine the second and third implementation. Luo [20] incorporates the body force $\vec{F}$ in the lattice Boltzmann method by adding the forcing term to the collision operator. When the body force $\vec{F}$ is uniform in space, the forcing term can be reduced as $\omega_i \rho \vec{e_i} \cdot \vec{F}/C_s^2$. But this reduction makes the work done by the body force disappear in the energy equation. Yet another form was proposed by Wolf-Gladrow [21], where the body force in the lattice Boltzmann method is incorporated by adding the forcing term to the collision operator.

Although force concept has been applied within the immersed boundary method, the methods are mostly implemented in the Navier-Stokes equation. In this paper, the lattice Boltzmann method is combined with the immersed boundary technique to simulate flows with moving curved boundary. The moving curved boundary is represented by a series of Lagrangian markers, and appropriate force is exerted at the Lagrangian markers to exactly satisfy the prescribed velocity. Then force at the Lagrangian markers is distributed to the Eulerian grid by a well-chosen discretized delta function. With the force known, the flow field can be obtained by the lattice Boltzmann method. Numerical examples are examined to investigate the capability of this approach.

II. The Lattice Boltzmann Method

A. Lattice Boltzmann Equation

The two dimensional lattice Boltzmann equation with BGK approximation and D2Q9 model can be expressed as,

$$f_i(\vec{x}+\vec{e}_i\Delta t, t+\Delta t) - f_i(\vec{x},t) = -\frac{1}{\tau}[f_i(\vec{x},t) - f_i^{eq}(\vec{x},t)], \tag{1}$$

where τ is the relaxation time and $i = 0 \sim 8$. The density, ρ, and the macroscopic flow velocity, $\vec{u} = (u_x, u_y)$, are defined in terms of the particle distribution function by

$$\rho = \sum_{i=0}^{8} f_i \tag{2}$$

$$\rho\vec{u} = \sum_{i=0}^{8} f_i \vec{e_i}. \tag{3}$$

The equilibrium distribution functions $f_i^{eq}(\vec{x},t)$ in D2Q9 model is defined as,

$$\begin{array}{l} f_i^{eq} = \omega_i \rho[1 + \frac{\vec{e}_i\cdot\vec{u}}{C_s^2} + \frac{(\vec{e}_i\cdot\vec{u})^2}{2C_s^4} - \frac{\vec{u}\cdot\vec{u}}{2C_s^2}] \\ \omega_0 = \frac{4}{9}, \omega_i = \frac{1}{9}, i = 1,2,3,4; \omega_i = \frac{1}{36}, i = 5,6,7,8. \end{array} \tag{4}$$

B. Lattice Boltzmann Method with Body Force Term

To combine the lattice Boltzmann method and the immersed boundary technique, the lattice Boltzmann equation with body force term $\vec{F} = (F_x, F_y)$[21] can be expressed as,

$$f_i(\vec{x}+\vec{e}_i\Delta t, t+\Delta t) = f_i(\vec{x},t) - \frac{1}{\tau}(f_i(\vec{x},t) - f_i^{eq}(\vec{x},t))$$

$$+\frac{1}{2}\frac{\omega_i}{C_s^2}[\vec{e}\cdot\vec{F}(\vec{x},t)] + \frac{1}{2}\frac{\omega_i}{C_s^2}[\vec{e}_i\cdot\vec{F}(\vec{x}+\vec{e}_i\Delta t, t+\Delta t)]\Delta t \tag{5}$$

Based on Eq. (5), the present lattice Boltzmann method is separated into three steps: the collision step, the streaming step and the forcing step for the moving curved boundary.

Collision step:

$$f_i'(\vec{x},t) = f_i(\vec{x},t) - \frac{1}{\tau}(f_i(\vec{x},t) - f_i^{eq}(\vec{x},t))$$

$$+\frac{1}{2}\frac{\omega_i}{C_s^2}[\vec{e}\cdot\vec{F}(\vec{x},t)]\Delta t \tag{6}$$

Streaming step:

$$f_i''(\vec{x}+\vec{e}_i\Delta t, t+\Delta t) = f_i'(\vec{x},t) \tag{7}$$

forcing step:

$$f_i(\vec{x}+\vec{e}_i\Delta t, t+\Delta t) = f_i''(\vec{x}+\vec{e}_i\Delta t, t+\Delta t)$$

$$+\frac{1}{2}\frac{\omega_i}{C_s^2}[\vec{e}_i\cdot\vec{F}(\vec{x}+\vec{e}_i\Delta t, t+\Delta t)]\Delta t \tag{8}$$

C. Forcing Step for the Moving Curved Boundary

The basis of the present immersed boundary method is based on the work of Su et al.[22], though it was derived from the Navier-Stokes equation framework. Here, the moving curved boundary is represented by a series of Lagrangian boundary markers $\vec{X}_k = (X_k, Y_k)$, and a force $\vec{F}_k = (X_{x,k}, Y_{y,k})$ is created on each Lagrangian boundary marker to ensure the satisfaction of the boundary condition. The force at the Lagrangian boundary marker $\vec{F}_k$ is distributed to the neighboring lattice by a well-chosen discretized delta function, and the boundary velocity is obtained by interpolation of velocity from its neighboring lattice. Here, the discretized delta function and the function responding for the interpolation of velocity are both set as the area-weighted average function δ_h:

$$\delta_h(\vec{x} - \vec{X}_k) = d_h(x_i - X_k)\, d_h(y_j - Y_k), \tag{9}$$

where d_h is the hat function and is defined by

$$d_h(r) = \begin{cases} (1 - |r|/h), & \text{for } |r| < h \\ 0, & \text{otherwise.} \end{cases} \tag{10}$$

where h is chosen as the lattice spacing Δx . The effective range of δ_h is a $2\Delta x$ by $2\Delta x$ square, and the maximum number of lattice influenced by a Lagrangian boundary marker is four. This function is in fact the bi-linear interpolation scheme.
The total force distributed to a lattice $\vec{F}(\vec{x})$ is the summation of weighted forces over the series of the Lagrangian boundary markers.

$$\vec{F}(\vec{x}) = \sum_k \vec{F}_k \cdot \delta(\vec{x} - \vec{X}_k) \tag{11}$$

where $\sum_k$ means the summation over the series of the Lagrangian boundary markers.
The velocity at a Lagrangian boundary marker $\vec{u}(\vec{X}_k)$ is the summation of weighted velocity over four neighboring lattice of the Lagrangian boundary marker $\vec{X}_k$.

$$\vec{u}(\vec{X}_k) = \sum_{\vec{x}} \vec{u}(\vec{x}) \cdot \delta(\vec{x} - \vec{X}_k) \tag{12}$$

where $\sum_{\vec{x}}$ means the summation over four neighboring lattice of the Lagrangian boundary marker $\vec{X}_k$.
The total force $\vec{F}(\vec{x})$ distributed to a lattice modifies its velocity by Eq. (8) so that the velocity at a Lagrangian boundary marker $\vec{u}(\vec{X}_k)$ obtained by interpolation exactly satisfies the prescribed velocity. ρ and $\rho\vec{u}$ at a lattice can be obtained by substituting Eq. (8) into Eq. (3), respectively.

III. Numerical Results

A. Lid-driven cavity

The lid-driven cavity flow is widely used to verify the accuracy of numerical method. In this test, the lid-driven cavity is inclined by 45 degree. Periodic boundary condition is imposed along the external boundary and the internal cavity boundary is prescribed using the immersed boundary technique. Fig. 1 shows the streamlines of the 45-degree-inclined lid-driven cavity within a square domain $[0, 2\sqrt{2}L] \times [0, 2\sqrt{2}L]$, where L is the width and height of the 45-degree-inclined lid-driven cavity. Three different uniform grids $(N \times N, N = 81, 161, 321)$ are used in the simulations with the corresponding number of Lagrangian markers $(NL = 4 \times 20, 4 \times 40, 4 \times 80)$, respectively. The Eulerian grid spacing is $\Delta x = \Delta y = 1/40$, the time step size is $\Delta t = \Delta x$, and the Reynolds number is $Re = 100$. The velocity of the driving lid is U, and the Mach number of the driving lid is $Mc = U/C_s = 0.1$. Since every boundary marker locates on a lattice, the Lagrangian marker spacing is $\Delta s = \sqrt{2}\Delta x$.

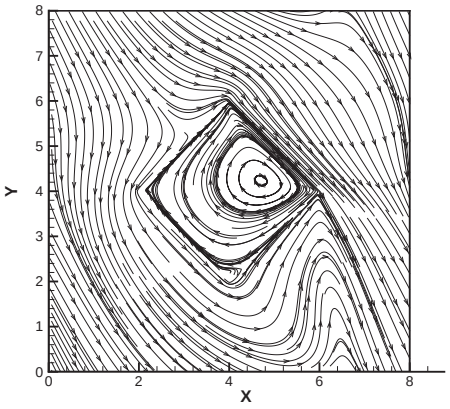

Fig. 1. The streamlines of the lid-driven cavity in the computational domain.

Fig. 2 shows the steady velocity component U inside the cavity but along the line $y = x$. The coordinate $Y = 0$ represents the intersection of the lower left edge and $y = x$. Fig. 3 shows the steady velocity component V inside the cavity but along the line $y = -x$. The coordinate $X = 0$ represents the intersection of the upper left edge and $y = -x$. We have shown all three numerical results calculated by different grids as well as the numerical result obtained by Ghia et al.[23]. One can see that our numerical results converge to the result obtained by Ghia et al. quite well.

B. steady uniform flow over a column of cylinders

This test is a uniform flow over a column of circular cylinders of radius r and center-to-center distance $H = 20r$.

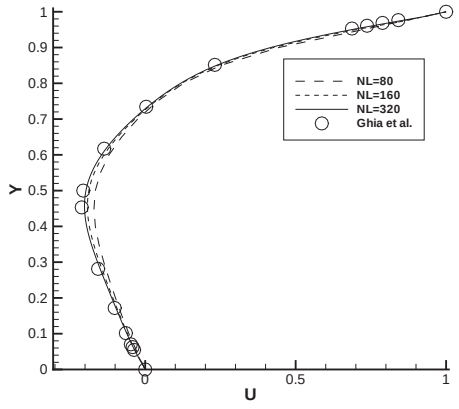

Fig. 2. The steady velocity component U along the line ($y = x$) through the center of cavity with different Eulerian grid sizes.

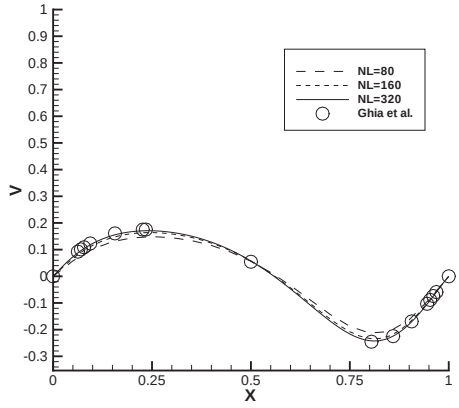

Fig. 3. The velocity component V along the central line ($y = -x$) through the center of cavity with different Eulerian grid sizes.

The center of the circular cylinder is located at $(0, H/2)$, and the radius of the circular cylinders is $r = 20\Delta x$. Periodic boundary conditions are prescribed along the upper and lower boundary at y=0 and H. The grid resolution in the y direction is $NJ = 401$. The Reynolds number is defined as $Re = 2rU/\nu = 100$, where U is the inlet velocity and this corresponds to a Mach number of $Mc = U/C_s = 0.1$. The velocity boundary condition in the inlet is implemented by Zou and He's method[24]. At the exit, the boundary condition for f_3, f_6 and f_7 are

$$f_i(NI, J) = f_i(NI - 1, J) for i = 3, 6 \; and \; 7 \qquad (13)$$

It must be noted that for a consistent determination of the force, the upstream boundary must be placed far upstream. A shorter distance between the cylinder and the boundary will result in higher drag. In this study, it is placed at 20 diameters to the left of the center of the cylinder. The downstream boundary is located 30 diameters behind the center of the cylinder to allow sufficient wake development. The grid resolution in the x direction is $NI = 2001$. The Eulerian grid spacing is $\Delta x = \Delta y = 1/40$, the time step size is $\Delta t = \Delta x$, and the number of Lagrangian markers is $NL = 160$.

Following Fornberg [25], the drag coefficient over the circular cylinder is defined as

$$C_D = \frac{F_D}{\rho_0 U^2 r} \qquad (14)$$

where F_D is the drag force obtained from

$$F_D = -\sum_k F_{x,k} \Delta x^2 \qquad (15)$$

And the lift coefficient over the circular cylinder is defined as

$$C_L = \frac{F_L}{\rho_0 U^2 r} \qquad (16)$$

where F_L is the lift force obtained from

$$F_L = -\sum_k F_{y,k} \Delta x^2 \qquad (17)$$

The result of Fornberg [25] shows that the flow is steady and the drag coefficient is 1.248. However, for Reynolds number over 47 the flow should be unsteady and vortex shedding occurs. Fig. 4(a) show the evolution of the drag and lift coefficients. The average value of C_D is 1.491 and its relative error is 19.47% compared to the result of Fornberg. Fig. 4(b)shows the instantaneous vorticity contours for $Re = 100$.

C. flow over an asymmetrically placed cylinder in a channel

Schafer and Turek [26] reported a set of benchmark results for a laminar flow over a circular cylinder of radius r that is asymmetrically placed inside a channel. In the present study, $r = 30\Delta x$ is used. The distance from the center of the cylinder to the upper wall and lower wall is $h^+ = 4.2r$ and $h^- = 4.0r$, respectively. The grid resolution in the y direction is $NJ = 247$. The channel inlet has a parabolic velocity profile of maximum speed U_max, and the Mach number of U_max is $Mc = U_max/Cs = 0.1$. No-slip boundary condition along the upper wall and the lower wall, and the parabolic velocity profile in the inlet are implemented by Zou and He's method. At the exit, the boundary condition for f_3, f_6 and f_7 is implemented by

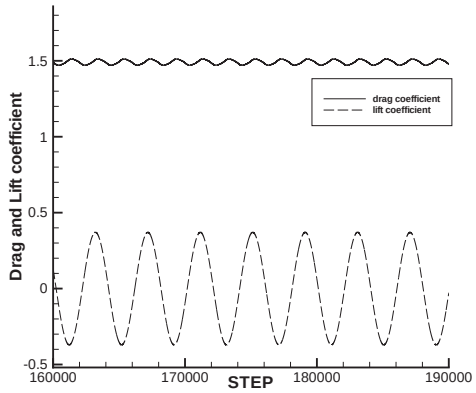

(a)

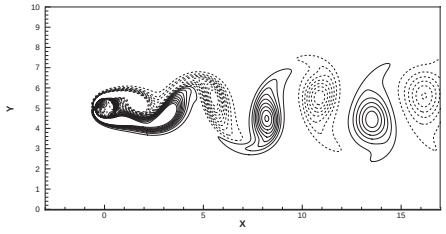

(b)

Fig. 4. (a) The step evolution of drag and lift coefficients of $Re = 100$. (b) The instantaneous vorticity contours near the cylinder; dotted and solid lines denote negative and positive contours.

Eq. (13). The inlet boundary is placed at 4 radii upstream of the cylinder center according to the specification of the benchmark test [26], and the exit boundary is located 40 radii downstream of the cylinder center. The grid resolution in the x direction is $NI = 1321$. The Eulerian grid spacing is $\Delta x = \Delta y = 1/40$, the time step size is $\Delta t = \Delta x$, and the number of Lagrangian markers is $NL = 240$.

The Reynolds number based on the average inlet velocity $U_{ave} = 2U_{max}/3$ is $Re = 2rU_{ave}/\nu = 100$. At this Reynolds number, the flow becomes unsteady and periodic vortex shedding is observed. The distribution functions are all initialized by the equilibrium distributions of constant density ρ_0 and parabolic velocity profile. The drag coefficient over the circular cylinder is defined as

$$C_D = \frac{F_D}{\rho_0 U_{ave}^2 r} \tag{18}$$

and the lift coefficient over the circular cylinder is defined as

$$C_L = \frac{F_L}{\rho_0 U_{ave}^2 r} \tag{19}$$

where the drag force F_D and the lift force F_L are obtained from Eq. (15) and Eq. (17), respectively.

Table I and Table II show the Values of C_D, C_L and St for the flow over a 2D cylinder asymmetrically placed in a channel at Re=20 and 100. One can see that the present results are compatible to those methods as mentioned in the introduction.

Figs. 5(a) and (b) show the lift and drag coefficients and instantaneous vorticty contours for Re=100. Table I and Table II show the Values of C_D, C_L and St for the flow over a 2D cylinder asymmetrically placed in a channel at Re=20 and 100. One can see that the present results are compatible to those methods as mentioned in the introduction. The predicted Strouhal number $St = 2r/U_{ave}T$ is 0.30027. This agrees very well with the range of Strouhal number (0.2950-0.3050) given in Ref. [26].

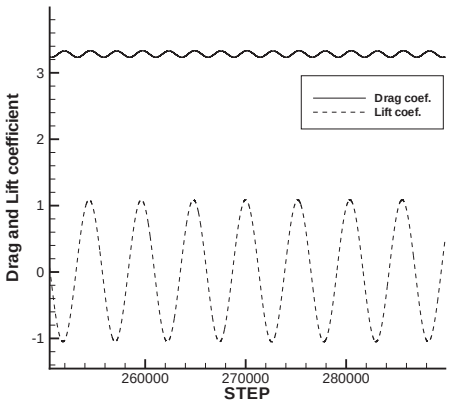

(a)

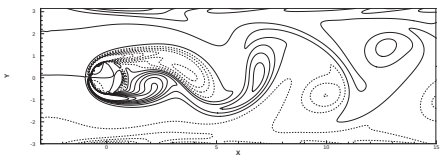

(b)

Fig. 5. (a) The time evolution of drag and lift coefficients of $Re = 100$. (b) The instantaneous vorticity contours near the cylinder; dotted and solid lines denote negative and positive contours.

TABLE I
VALUES OF C_D, C_L AND St FOR THE FLOW OVER A 2D CYLINDER ASYMMETRICALLY PLACED IN A CHANNEL AT RE=20.

	Present	Shyy et al.[27]	Schafer & Turek [26]
C_D	5.679	5.59	5.57 - 5.59
C_L	0.0114	-	0.0104 - 0.0110

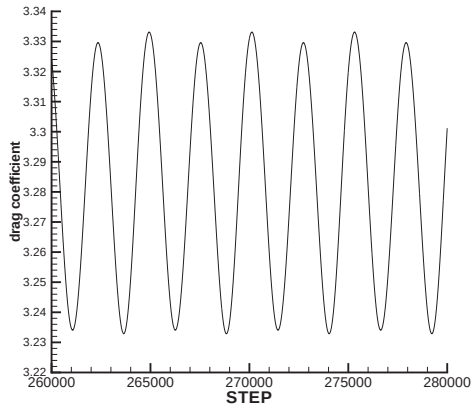

Fig. 6. The time evolution of drag coefficients of $Re = 100$.

TABLE II
VALUES OF C_D, C_L AND St FOR THE FLOW OVER A 2D CYLINDER ASYMMETRICALLY PLACED IN A CHANNEL AT RE=100.

	Present	Shyy et al. (Stress)[28]	Schafer & Turek [26]
C_D	3.333	3.2275	3.22 - 3.24
C_L	1.0511	1.0040	0.99 - 1.01
St	0.3002	0.3033	0.295 - 0.305

D. Galilean invariance

Here, Galilean invariance of the proposed method is examined. The flow simulation is performed in two frames of reference. First, the cylinder is moving at a constant velocity $(U, 0)$ with respect to the computational domain, and the wall of the channel is fixed. Second, the position of the cylinder is fixed on the computational domain, and the wall of the channel is moving at a constant velocity $(-U, 0)$. The relative motion between the cylinder and the flow in the channel should remain the same in either case. Periodic boundary conditions are applied at the inlet and outlet and the velocity boundary condition for the wall of the channel is implemented by Zou and He's method.

The circular cylinder is modeled by Lagrangian markers, where the number of Lagrangian markers is $NL = 78$. The radius of the circular cylinder is $r = 10\Delta x$ and the characteristic speed U is $\frac{1}{18}\frac{\Delta x}{\Delta t}$. Therefore, the Reynolds numner based on the radius of the circular cylinder is $Re = Ur/\nu = 12.5$. The Eulerian grid spacing is $\Delta x = \Delta y = 1/40$, and the time step size is $\Delta t = \Delta x$. The length and the height of the computational domain is $22r$ and $6r$, respectively. The circular cylinder is initially located at the center of the computational domain, and the number of time steps is 396000.

The streamwise velocity component for the moving cylinder flow is denoted as $u_{cylinder}$ and the streamwise velocity component for the moving channel flow is assigned as $u_{channel}$. The relationship between these two frames of reference is

$$u_{channel} = u_{cylinder} - U \tag{20}$$

Fig. 7 and 8 show the streamlines for the moving cylinder flow and the moving channel flow, the contour for $u_{cylinder} - U$ and $u_{channel}$, respectively. Based on these two figures, it is observed that Eq. (20) is actually satisfied. Hence the Galilean invariance for the lattice Boltzmann method with our immersed boundary technique is ensured.

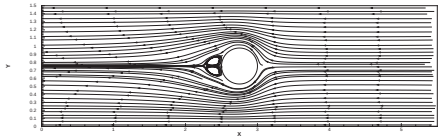

Fig. 7. The streamlines for a moving cylinder in a fixed channel

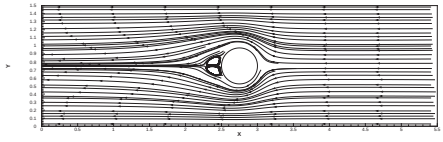

Fig. 8. The streamlines for a fixed cylinder in a moving channel

IV. CONCLUSION

The lattice Boltzmann method is combined with the immersed boundary technique to simulate flows with moving curved boundary. A moving curved boundary is represented by a series of Lagrangian markers, and appropriate force is exerted at the Lagrangian markers to exactly satisfy the prescribed velocity. Then force at the Lagrangian markers is distributed to the Eulerian grid by a well-chosen discretized delta function. Lattice Boltzmann method with the forcing term is used to obtain the velocity field. The proposed method is examined by computing lid driven cavity flow and flows over both stationary and moving cylinder. All the numerical results agree well with the analytical solution or the benchmark solution, and the Galilean invariance is satisfied.

REFERENCES

[1] U. Frisch, B. Hasslacher, and Y. Pomeau, Phys. Rev. Lett. 56,1505 (1986); S. Wolfram, J. Stat. Phys. 45, 471 (1986).

[2] F. J. Higuera, S. Succi, and R. Benzi, Europhys. Lett. 9, 345 (1989); F. J. Higuera and J. Jeme?nez, ibid. 9, 663 (1989).

[3] P. L. Bhatnagar, E. P. Gross, and M. Krook, Phys. Rev. 94, 511 (1954).

[4] S. Harris, "An Introduction to the Theory of the Boltzmann Equation", Holt, Rinehart and Winston, New York, (1971).

[5] H. Chen, S. Chen, and W. H. Matthaeus, Phys. Rev. A 45, R5339 (1991); Y. H. Qian, D. d'Humie'res, and P. Lallemand, Europhys. Lett. 17, 479 (1992).

[6] U. Frisch, D. d'Humi?res, B. Hasslacher, P. Lallemand, Y. Pomeau, and J.-P. Rivet, "Lattice gas hydrodynamics in two and three dimensions", Complex Syst. 1, 649 (1987).

[7] D. O. Martinez, W. H. Matthaeus, S. Chen, and D. C. Montgomery, "Comparison of spectral method and lattice Boltzmann simulations of two-dimensional hydrodynamics", Phys. Fluids 6, 1285 (1994).

[8] O. Filippova, D. H?nel, "Grid refinement for lattice-BGK models", J. Comput. Phys. 147, 219 (1998).

[9] R. Mei, L.-S. Luo, W. Shyy, "An Accurate Curved Boundary Treatment in the Lattice Boltzmann Method", J. Comput. Phys. 155, 307 - 330 (1999).

[10] P. Lallemand, L.-S. Luo, "Lattice Boltzmann method for moving boundaries", J. Comput. Phys. 184, 406 - 421 (2003).

[11] M. Bouzidi, M. Firdaouss, P. Lallemand, "Momentum transfer of a lattice-Boltzmann fluid with boundaries", Phys. Fluids 13, 3452 - 3459 (2002).

[12] C. S. Peskin, "Flow patterns around heart valves: a numerical method", J. Comp. Phys. 10, 252 (1972).

[13] M.-C. Lai and C. S. Peskin, "An immersed boundary method with formal second order accuracy and reduced numerical viscosity", J. Comp. Phys. 160, 705 (2000).

[14] D. Goldstein, R. Handler, and L. Sirovich, "Modeling a no-slip flow with an external force field", J. Comp. Phys. 105, 354 (1993).

[15] D. Goldstein, R. Hadler, L. Sirovich, "Direct numerical simulation of turbulent flow over a modeled riblet covered surface", J. Fluid Mech. 302, 333. (1995).

[16] E. M. Saiki, and S. Biringen, "Numerical simulation of a cylinder in uniform flow: application of a virtual boundary method", J. Comp. Phys. 123, 450 (1996).

[17] J. Mohd-Yusof, "Combined immersed boundary/ B-Spline method for simulations of flows in complex geometries", CTR Annual Research Briefs, NASA Ames/ Stanford University, (1997).

[18] E. A. Fadlun, R. Verzicco, P. Orlandi, and J. Mohd-Yusof, "Combined immersed-boundary methods for three dimensional complex flow simulations", J. Comp. Phys. 161, 30 (2000).

[19] J. M. Buick and C. A. Greated, "Gravity in a lattice Boltzmann model", Physical Review E, 61, NUMBER 5, (MAY 2000).

[20] Li-Shi Luo, "Theory of the lattice Boltzmann method: Lattice Boltzmann models for nonideal gases", Physical Review E, 62, NUMBER 4, (OCTOBER 2000).

[21] Dieter A. Wolf-Gladrow, "Lattice-Gas Cellular Automata and Lattice Boltzmann Models - An Introduction", Springer, Berlin, Lecture Notes in Mathematics (2000).

[22] Shen-Wei Su, Ming-Chih Lai, Chao-An Lin, "A simple immersed boundary technique for simulating complex flows with rigid boundary", submitted to J. Comp. Phys. 34. Bengt Fornberg, "Steady

[23] U. Ghia, K. N. Ghia, and C. T. Shin, "High-Re solutions for incompressible flow using the Navier-Stokes Equations and a multi-grid method", J. Comp. Phys. 48, 387 (1982).

[24] Q. Zou, X. He, "On pressure and velocity boundary conditions for the lattice Boltzmann BGK model", Phys. Fluids 9, 1591 - 1598 (1997).

[25] Bengt Fornberg, "Steady incompressible flow past a row of circular cylinders", J. Fluid Mech. 225, 655 (1991).

[26] M. Schafer and S. Turek, in "Flow Simulation with High-Performance Computer II", edited by E. H. Hirschel, Notes in Numerical Fluid Mechanics (Vieweg, Braunschweig, 1996), 52, 547-566

[27] D. Yu, R. Mei, and W, Shyy, "Viscous flow computations with the method of lattice Boltzmann eqution", Progress in Aerospace Sciences. 39, 329-367 (2003).

[28] R. Mei, D. Yu, and W. Shyy, "Force evaluation in the lattice Boltzmann method involving curved geometry", Phys. Rev. E 65, 041203